Numerical dispersion effects on the energy cascade in large-eddy simulation

Gopal R. Yalla,[1] Todd A. Oliver,[1] and Robert D. Moser[1,2]

[1] *The Oden Institute for Computational Engineering and Sciences, The University of Texas at Austin*
[2] *Department of Mechanical Engineering, The University of Texas at Austin*

Implicitly filtered Large Eddy Simulation (LES) is by nature numerically under-resolved. With the sole exception of Fourier-spectral methods, discrete numerical derivative operators cannot accurately represent the dynamics of all of the represented scales. Since the resolution scale in an LES usually lies in the inertial range, these poorly represented scales are dynamically significant and errors in their dynamics can affect all resolved scales. This Letter is focused on characterizing the effects of numerical dispersion error by studying the energy cascade in LES of convecting homogeneous isotropic turbulence. Numerical energy and transfer spectra reveal that energy is not transferred at the appropriate rate to wavemodes where significant dispersion error is present. This leads to a deficiency of energy in highly dispersive modes and an accompanying pile up of energy in the well resolved modes, since dissipation by the subgrid model is diminished. An asymptotic analysis indicates that dispersion error causes a phase decoherence between triad interacting wavemodes, leading to a reduction in the mean energy transfer rate for these scales. These findings are relevant to a wide range of LES, since turbulence commonly convects through the grid in practical simulations. Further, these results indicate that the resolved scales should be defined to not include the dispersive modes.

In numerical analysis, one generally aspires to make the resolution sufficiently fine so that discretization error is negligible. However, Large Eddy Simulation (LES) is, by definition, under-resolved. In practice, information about the small-scale turbulence is discarded by numerical discretization. This includes the projection of the infinite-dimensional velocity field onto a finite-dimensional solution space (often referred to as the implicit filter) and the introduction of numerical derivative operators, which together characterize the scales in the resolved field whose dynamics are accurately represented. Since the resolution scale in an LES often lies in the energy-containing inertial range, the effects of discretization error must generally be considered, with the sole exception being for Fourier-spectral methods. In this Letter, we examine the statistical consequences of this dispersion error in LES.

A simple flow in which to explore these dispersion error effects is infinite Reynolds number forced homogeneous isotropic turbulence with fluctuating velocities $\mathbf{u}$ transported with a uniform convection velocity $\mathbf{U}$, with magnitude U. We consider an LES with homogeneous isotropic resolution Δ, and following Moser *et al.* [1] write the filtered incompressible Navier-Stokes equations for the fluctuating velocity for this case as

$$\frac{\partial \overline{u}_i}{\partial t} + U_j \frac{\delta \overline{u}_i}{\delta x_j} + \frac{\delta \mathcal{F}(\overline{u}_i \overline{u}_j)}{\delta x_j} = -\frac{\delta \bar{p}}{\delta x_i} + \frac{\delta \tau_{ij}}{\delta x_j} - \mathcal{C}_i^m + f_i \tag{1}$$

$$\frac{\delta \overline{u}_i}{\delta x_i} = -\mathcal{C}^c. \tag{2}$$

where p is the pressure, f_i is the forcing, $\bar{\cdot}$ designates a filtered quantity, $\mathcal{F}(\cdot)$ is a (potentially different) filtering operator that maps the nonlinear terms to the LES solution space, and $\tau_{ij} = -\overline{u_i u_j} + \mathcal{F}(\overline{u}_i \overline{u}_j)$ is the subgrid stress. Furthermore, $\delta/\delta\mathbf{x}$ denotes the discrete derivative operator. The terms $\mathcal{C}_i^m$ and $\mathcal{C}^c$ are generalized commutators [2] that, in this case, solely account for the discretization errors in the numerical derivatives. More generally, they represent the difference between the exact terms in the filtered equations and the approximate terms used in the LES computations. The approximations to the pressure gradient and continuity equation are not of interest here. Instead we focus on the linear and nonlinear convective terms and their contributions $\mathcal{C}_i^l$ and $\mathcal{C}_i^n$, respectively, to the generalized commutator $\mathcal{C}_i^m$, where:

$$\mathcal{C}_i^l = U_j \left(\overline{\frac{\partial u_i}{\partial x_j}} - \frac{\delta \overline{u}_i}{\delta x_j} \right) \qquad \mathcal{C}_i^n = \overline{\frac{\partial \mathcal{F}(\overline{u}_i \overline{u}_j)}{\partial x_j}} - \overline{\frac{\partial \tau_{ij}}{\partial x_j}} - \frac{\delta \mathcal{F}(\overline{u}_i \overline{u}_j)}{\delta x_j} + \frac{\delta \tau_{ij}}{\delta x_j} \tag{3}$$

Usually, these commutators are neglected in an LES.

To assess the consequences of neglecting $\mathcal{C}_i^m$, we solve (1) and (2) assuming $\mathcal{C}_i^m = 0$ for forced homogeneous isotropic turbulence with periodic boundary conditions. Both filters $\bar{\cdot}$ and $\mathcal{F}(\cdot)$ are defined to be Fourier cutoff filters, to allow us to isolate dispersion effects from aliasing effects. However, simulations using a collocation projection for $\mathcal{F}$ yielded results similar to those presented here.

Six different discrete first derivative operators $\delta/\delta\mathbf{x}$ are used: a Fourier-spectral method, a 2nd order centered difference method, and 2nd, 3rd, 4th, and 7th order B-spline collocation methods. All the operators are implemented in a modified version of the Fourier spectral code POONGBACK [3] by substituting the effective wavenumbers associated

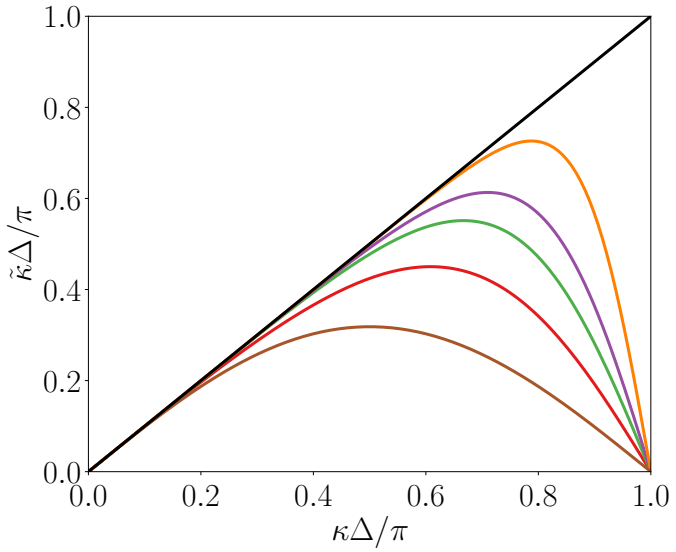

FIG. 1: The effective wavenumbers corresponding to the first derivative operators for a Fourier-spectral method (———), 7th order B-spline collocation method (———), 4th order B-spline collocation method (———), 3rd order B-spline collocation method (———), 2nd order B-spline collocation method (———), and 2nd order centered difference method (———).

with each method for the true wavenumber when evaluating first derivatives in Fourier-space. Specifically, let $i\tilde{\kappa}(\kappa)$ be the eigenvalue of the first numerical derivative operator that corresponds to the eigenfunction $e^{i\kappa x}$. Then $\tilde{\kappa}$ is the effective wavenumber for the first derivative operator, which is plotted in Figure 1 for the numerical derivative operators of interest here. The effective wavenumber for the first derivative in the i^{th} coordinate direction is then $\tilde{\kappa}_i = \tilde{\kappa}(\kappa_i)$ and an effective wave "vector" $\tilde{\boldsymbol{\kappa}}$ can be defined with components $\tilde{\kappa}_i$. To isolate the effects of numerical dispersion, the Laplacian that arises from the eddy viscosity model for the subgrid stress because ν_t is a constant (see below) is treated spectrally in all the LES performed here.

A third-order low storage Runge-Kutta method [4] is used for time advancement, with time step selected to maintain CFL=0.5 as defined in Spalart *et al.* [4]. The filtered Navier-Stokes equations are solved using the vorticity-velocity formulation of Kim *et al.* [5]; see Appendix 1 for more details regarding the implementation of the vorticity-velocity formulation for non-spectral numerics. The skew-symmetric form of the nonlinear terms is used in the LES because it conserves both momentum and energy and has been reported to perform well in the presence of aliasing and discretization errors in LES [6–9]. In addition, the consequences of dispersion error in other forms of the nonlinear terms are discussed.

The forcing f_i is formulated to inject energy at a constant rate ε as in [10] and the simulations are performed in a cubical domain of size L. Because the turbulence is statistically stationary, ε is also the mean rate of kinetic energy dissipation. Unless otherwise indicated, all quantities are reported in units in which $\varepsilon = 1$ and $L = 2\pi$. The filtered velocity is represented with 32 Fourier modes in each direction, for an effective uniform resolution of $\Delta = 2\pi/32$, and the forcing f_i is active only in the wavenumber range $0 < |\boldsymbol{\kappa}| \leq 2$. The filter $\mathcal{F}(\cdot)$ (a Fourier cutoff) is applied to the nonlinear terms as in a dealiased pseudo-spectral method, by evaluating the nonlinear product on a 48^3 grid and truncating the discrete Fourier transform of the result to 32^3 Fourier modes (the 3/2 rule) [11]. The subgrid stress is approximated by a Kolmogorov model $\tau_{ij} = 2\nu_t S_{ij}$, where $\nu_t = C_m \Delta^{4/3} \varepsilon^{1/3}$, is the eddy viscosity, $S_{ij} = \frac{1}{2}(\delta_i \bar{u}_j + \delta_j \bar{u}_i)$ is the filtered strain rate tensor and $C_m = 0.065$ [12, 13]. Note that the phenomenon reported here is not dependent on this choice of the subgrid model. In particular, similar results are obtained using models with a fluctuating eddy viscosity, such as the Smagorinsky model.

Letting $\hat{\cdot}$ denote the Fourier transform and $\cdot^*$ denote the complex conjugate, the evolution equation for the instantaneous resolved energy spectrum $E(\boldsymbol{\kappa}, t) = \frac{1}{2}\hat{\bar{u}}_j^*(\boldsymbol{\kappa}, t)\hat{\bar{u}}_j(\boldsymbol{\kappa}, t)$ in the LES is

$$\frac{\partial E(\boldsymbol{\kappa}, t)}{\partial t} = T_{\text{N}}(\boldsymbol{\kappa}, t) - 2\nu_t |\boldsymbol{\kappa}|^2 E(\boldsymbol{\kappa}, t) + F(\boldsymbol{\kappa}, t), \tag{4}$$

where T_{N} is the numerical transfer spectrum that represents the exchange of energy between wavenumbers due to triad interactions, in the presence of numerical dispersion error, and $F = \text{Re}\left\{\hat{\bar{u}}_j^*(\boldsymbol{\kappa}, t)\hat{f}_j(\boldsymbol{\kappa}, t)\right\}$ is the spectrum of the energy production arising from the forcing. For the skew-symmetric form of the nonlinear terms used here, $T_{\text{N}} = T_{\text{skew}}$

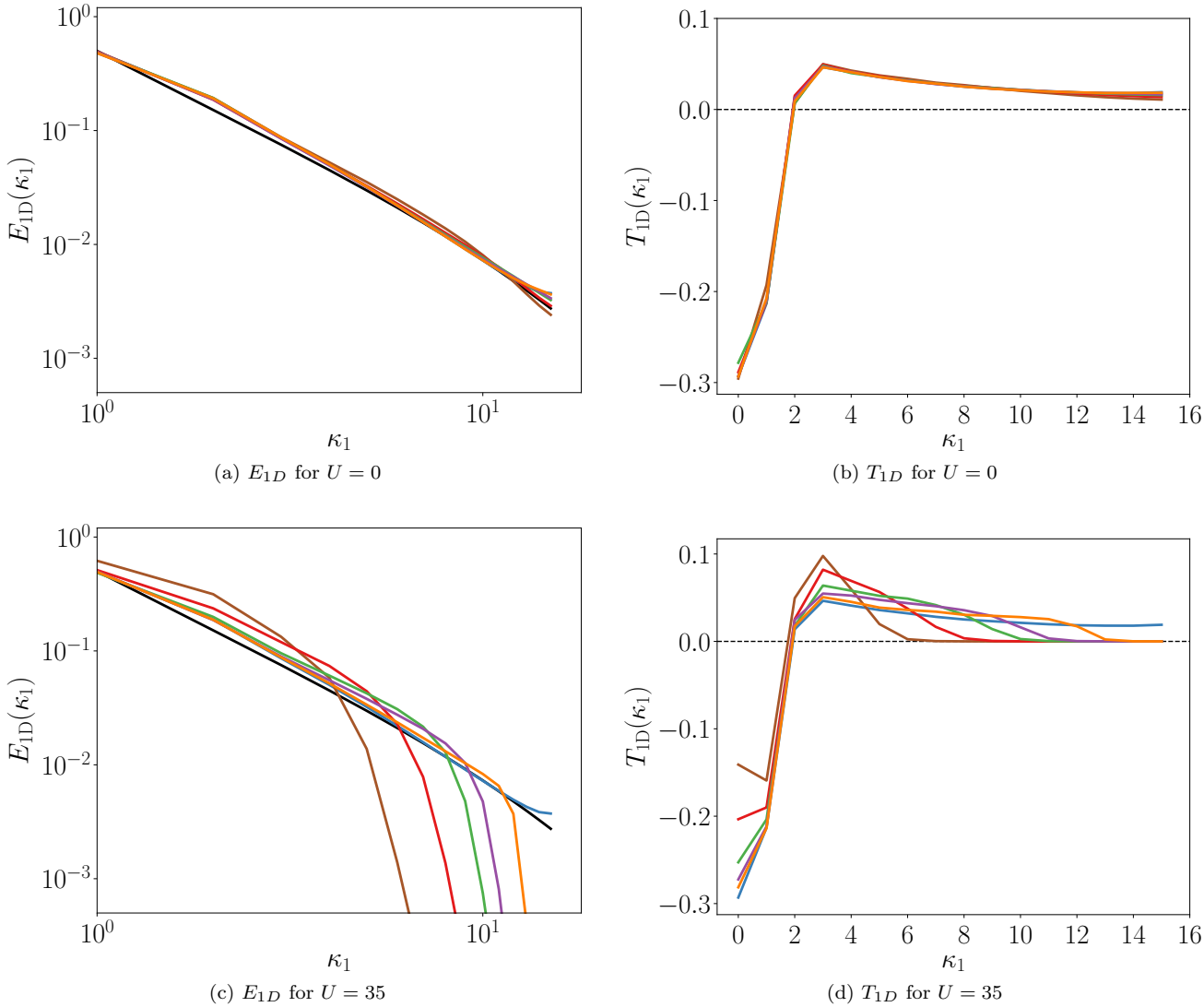

(a) E_{1D} for $U = 0$

(b) T_{1D} for $U = 0$

(c) E_{1D} for $U = 35$

(d) T_{1D} for $U = 35$

FIG. 2: One dimensional spectra in the convection direction of energy E_{1D} and energy transfer rate T_{1D}, with convection velocities $U = 0$ and 35. Shown are spectra from theory (——), Fourier-spectral method (——), 7th order B-spline collocation method (——), 4th order B-spline collocation method (——), 3rd order B-spline collocation method (——), 2nd order B-spline collocation method (——), 2nd order centered difference method (——).

with

$$T_{\text{skew}}(\boldsymbol{\kappa}, t) = -\frac{1}{2}\text{Im}\left\{\sum_{\boldsymbol{\kappa}'}(\tilde{\kappa_\ell'} + \tilde{\kappa}_\ell)\hat{\tilde{u}}_k(\boldsymbol{\kappa}, t)\hat{\tilde{u}}_k^*(\boldsymbol{\kappa}', t)\hat{\tilde{u}}_\ell^*(\boldsymbol{\kappa} - \boldsymbol{\kappa}', t)\right\}. \tag{5}$$

See Appendix 2 for further discussion of the transfer spectrum for this and other nonlinear forms. The LES results reported here are the one-dimensional energy spectra in the direction of the convection velocity, which is chosen to be aligned with the grid direction ($i = 1$). The energy spectra are computed as $E_{1D}(\kappa_1) = \sum_{\kappa_2,\kappa_3}\langle E(\boldsymbol{\kappa}, t)\rangle$, where $\langle\cdot\rangle$ indicates the expected value, which is approximated as a time average. In addition, analogous one-dimensional transfer spectra $T_{1D}(\kappa_1) = \sum_{\kappa_2,\kappa_3}\langle T_{\text{skew}}(\boldsymbol{\kappa}, t)\rangle$ are reported. When the convection velocity is not aligned with the grid, dispersive effects on the one-dimensional spectra similar to those reported here occur in each grid direction in which $\mathbf{U}$ has a non-zero component.

In the absence of mean convection ($U = 0$), each numerical scheme produces spectra that agree with an equivalently filtered $\kappa^{-5/3}$ theoretical inertial range spectrum (see Figure 2a). Furthermore, the transfer spectra are identical to that for the Fourier-spectral case for all the numerical approximations (see Figure 2b). For reference, the statistical characteristics of the turbulence for the $U = 0$, Fourier-spectral case are reported in Table I.

TABLE I: Statistical characteristics of LES turbulence averaged over 500 eddy turnover times for the $U = 0$ case with Fourier spectral numerics. Values are normalized by ε and $L/2\pi$.

Resolved Kinetic Energy, $k_{res} = \frac{1}{2}\langle \bar{u}_i \bar{u}_i \rangle$	2.467
RMS Velocity, $u' = \sqrt{(2/3)k_{res}}$	1.282
Integral Scale, $\mathcal{L} = \frac{\pi E_{1D}(0)}{u'^2}$	1.129
Large Eddy Turnover Time, $T_L = \mathcal{L}/u'$	0.880

To demonstrate numerical dispersion effects, consider the case with mean convection velocity $U = 35$. In this case, the value of $U/u' \approx 27$ (u' is the standard deviation or root-mean square of a velocity component, and is defined in Table I) is comparable to that at the centerline of a turbulent channel flow, where U/u' ranges from 23 to 30 for friction Reynolds number ranging from 180 to 5200 [3]. As expected, for spectral numerics, no change from the $U = 0$ case occurs in either the energy spectrum or transfer spectrum. However, for all other numerical schemes, the one-dimensional energy spectra in the direction of convection are significantly reduced over a range of the highest resolved wavenumbers (see Figure 2c). The corresponding transfer spectra in the direction of convection tend to zero over this range of resolved modes (see Figure 2d). In effect, numerical dispersion error prevents energy from transferring at the appropriate rate from the largest to smallest resolved scales. As a consequence, energy also piles up in the larger resolved scales as energy is not transferred to the smallest resolved scales at the correct rate for the subgrid model to dissipate (see Figure 2c). For energy conserving numerics, we must have $\sum_{\boldsymbol{\kappa}} T_{\mathrm{N}}(\boldsymbol{\kappa}, t) = 0$ for all t. To maintain this balance, the energy transfer spectrum at all wavenumbers is affected by the dispersion error that is primarily in the largest wavenumbers (see Figure 2d). Moreover, the energy transfer rates in directions orthogonal to convection are not degraded, however, the nonphysical effects of numerical dispersion on energy transfer in the convection direction also impact the energy spectra in the orthogonal directions (not shown).

The reason for the observed degradation of energy transfer to the smallest resolved scales when $U > 0$ can be understood through analysis of a case in which $U \gg u'$. Let $\epsilon = u'/U \ll 1$ be a small parameter (not to be confused with the mean dissipation rate ε). Then the velocity Fourier coefficients $\hat{\bar{u}}_i$ vary on a fast and a slow time scale. Using a multiscale asymptotic representation, $\hat{\bar{u}}_i$ can be said to depend on a fast time variable $t_f = t/\epsilon$ and a slow time variable $t_s = t$. Further, as with Taylor's hypothesis, in the continuous case, $\partial/\partial t_f = \epsilon U_j \partial/\partial x_j$ is order one in ϵ. But, when using discrete derivatives as in (1), the same analysis yields $\partial/\partial t_f = \epsilon U_j \delta/\delta x_j$. Therefore, $\hat{\bar{u}}_i$ can be written:

$$\hat{\bar{u}}_i(\boldsymbol{\kappa}, t_f, t_s) = \hat{\bar{u}}_i(\boldsymbol{\kappa}, t_s) e^{-i\epsilon \mathbf{U}\cdot\tilde{\boldsymbol{\kappa}} t_f} + \mathcal{O}(\epsilon) \tag{6}$$

where $\hat{\bar{u}}_i(\boldsymbol{\kappa}, t_s)$ is simply the fast time average of $\hat{\bar{u}}_i$, which varies in slow time due to the nonlinear turbulent processes. The instantaneous energy transfer rate for this skew-symmetric form as used here (5) is then

$$T_{\mathrm{skew}}(\boldsymbol{\kappa}, t_f, t_s) = -\frac{1}{2}\mathrm{Im}\left\{ \sum_{\boldsymbol{\kappa}'} (\widetilde{\kappa'_\ell} + \tilde{\kappa}_\ell) \hat{\bar{u}}_k(\boldsymbol{\kappa}, t_s) \hat{\bar{u}}^*_k(\boldsymbol{\kappa}', t_s) \hat{\bar{u}}^*_\ell(\boldsymbol{\kappa} - \boldsymbol{\kappa}', t_s) e^{i\epsilon \mathbf{U}\cdot(\tilde{\boldsymbol{\kappa}}' - \tilde{\boldsymbol{\kappa}} - \widetilde{(\boldsymbol{\kappa}' - \boldsymbol{\kappa})}) t_f} \right\} + \mathcal{O}(\epsilon) \tag{7}$$

Since the turbulence is assumed to be stationary and ergodic, the expected value $\langle T(\boldsymbol{\kappa}) \rangle$ is time independent and can be estimated as a time average as follows:

$$\langle T_{\mathrm{skew}}(\boldsymbol{\kappa}) \rangle = -\frac{1}{2}\mathrm{Im}\left\{ \sum_{\boldsymbol{\kappa}'} (\widetilde{\kappa'_\ell} + \tilde{\kappa}_\ell) \langle \hat{\bar{u}}_k(\boldsymbol{\kappa}, t_s) \hat{\bar{u}}^*_k(\boldsymbol{\kappa}', t_s) \hat{\bar{u}}^*_\ell(\boldsymbol{\kappa} - \boldsymbol{\kappa}', t_s) \rangle \left\langle e^{i\epsilon \mathbf{U}\cdot(\tilde{\boldsymbol{\kappa}}' - \tilde{\boldsymbol{\kappa}} - \widetilde{(\boldsymbol{\kappa}' - \boldsymbol{\kappa})}) t_f} \right\rangle_{t_f} \right\} + \mathcal{O}(\epsilon) \tag{8}$$

where $\langle \cdot \rangle_{t_f}$ is the fast time average, and the (slow) time average of the $\hat{\bar{u}}_i$ triple product has been replaced by the expected value by ergodicity.

Clearly, the fast time average in (8) is zero unless

$$\omega_T = \mathbf{U} \cdot (\tilde{\boldsymbol{\kappa}}' - \tilde{\boldsymbol{\kappa}} - \widetilde{(\boldsymbol{\kappa}' - \boldsymbol{\kappa})}) = 0, \tag{9}$$

in which case it is one. When using Fourier spectral numerics, $\tilde{\boldsymbol{\kappa}} = \boldsymbol{\kappa}$ and (9) is satisfied identically for all the triad interactions represented in (8). However, for other numerical schemes, such as those analyzed in Fig. 1, $\tilde{\boldsymbol{\kappa}}$ is a nonlinear function of $\boldsymbol{\kappa}$, and so (9) will generally not be satisfied unless $|\mathbf{U} \cdot \boldsymbol{\kappa}| = |\mathbf{U} \cdot \boldsymbol{\kappa}'|$, severely limiting the

triad interactions that contribute to net energy transfer among wavenumbers. This occurs because the spatial Fourier modes that can interact to transfer energy are determined by the wavenumbers $\boldsymbol{\kappa}$, while the convective dynamics of those modes are determined by $\tilde{\boldsymbol{\kappa}}$. The result is that the interacting wavemodes do not maintain consistent phase relationships, essentially shutting down the energy transfer and producing spectral anomalies like those shown in Fig. 2. The inhibition of energy transfer due to phase scrambling discussed here is similar to that caused by rapid rotation as described, for example, in [14, 15].

Of course, this analysis is asymptotic for $\epsilon \to 0$. For any finite ϵ, there will be $\mathcal{O}(\epsilon)$ corrections because the phase scrambling effect of the mean convective dispersion errors as described above will compete with the nonlinear evolution of the Fourier modes. In this case, one would expect that triad interactions for which $\omega_T \neq 0$ in (9) would be weakened, rather than completely excluded, depending on the magnitude of ω_T. This may be the reason the spectra in Fig. 2 roll off smoothly for wavenumbers with significant dispersion error.

The condition (9) suggests that the strength of the dispersion effect on the energy transfer at any wavenumber is determined by $U(\kappa - \tilde{\kappa}) = U\Delta\kappa$, which measures the rapidity of the phase scrambling. Provided $U\Delta\kappa$ at some wavenumber is sufficiently small compared to the rate of other processes, one would expect the dispersion effects on the energy transfer at that wavenumber to be negligible. This is supported by the observation that, for the third, fourth and seventh order B-splines [16], the value of $\Delta\kappa$ at the wavenumbers where the transfer spectrum crosses that for spectral numerics in Figure 2d is approximately the same (~ 0.4). In addition, in simulations with convection velocity increased (decreased) by a factor of two (not shown), $\Delta\kappa$ at this cross-over is decreased (increased) by about a factor of two.

While the above analysis was performed for the skew-symmetric form of the nonlinear terms, the structure of the transport spectrum is similar for other forms (see Appendix 2), and the same analysis applies. This suggests that the same dispersion effects should occur for the convective, conservative and rotational form of the nonlinear terms, and this was confirmed numerically. Furthermore, as is well known, the convective and conservative forms do not necessarily conserve energy in the presence of discretization error. Like the mean convective dispersion, this failure of energy conservation is driven by the fact that $\tilde{\boldsymbol{\kappa}}' - \tilde{\boldsymbol{\kappa}} - \widetilde{(\boldsymbol{\kappa}' - \boldsymbol{\kappa})} \neq 0$ (Appendix 2), which distorts the energy spectrum even when $U = 0$. However, when $U \gg u'$, dispersion due to mean convection dominates, and the results are similar to those presented here for the skew-symmetric form.

DISCUSSION

In many LES applications, the turbulence is convected with a velocity large compared to the turbulence fluctuations (e.g., turbulent boundary layers [17], flow through a wind turbine [18]). In LES of such turbulent flows, numerical dispersion error causes a decoherence of the phase relationship among interacting Fourier modes, which results in a reduction of the energy transfer rate from large to small resolved scales in the direction of convection. This leads to nonphysical changes in the energy distribution across all resolved scales.

On the other hand, the $U = 0$ results indicate that the nonlinear dispersion error has little effect on the LES spectra, despite an inaccurate representation of the resolved scale dynamics (see Figures 2a and 2b). This is interesting because one might expect the energy transfer to be affected by phase scrambling due to convection of the small scales by the large scales even when $U = 0$. By analogy with the scaling with the mean convection velocity, the strength of this effect should scale with u' so that, provided $u'\Delta\kappa$ is sufficiently small compared to the rate of other processes, the impact of dispersion on energy transfer should be negligible. Presumably this is the case for all scales in the $U = 0$ simulations shown in Figure 2.

However, the good $U = 0$ results presented here should be interpreted with caution, since the highly dispersive scales can have a damaging effect in more complex flows [2, 8, 19, 20]. Consequently, in an LES, we generally cannot expect the scales with significant dispersion error to be dynamically meaningful.

There are two potential approaches to addressing the consequences of dispersion error in LES. First, one could introduce a model for $\mathcal{C}_i^m$ in equation (1) to correct for the dispersion effects. However, it is not clear that such a model can be formulated. Alternatively, one could define the large scales being simulated to only include those with sufficiently small dispersion errors. However, the standard for sufficiently small dispersion error depends on the convection velocity and possibly other flow characteristics, not just the characteristics of the derivative approximation.

In one approach, the large scales to be simulated can be defined using an explicit filter, acting in addition to the implicit filter defined by the numerical discretization, to ensure that the scales with significant dispersion error are not energized [21–30], and this was found to be effective. But such explicit filters are commonly not used so as to maximize the range of scales being represented. In this case, when interpreting the results one should still discount the overly dispersive scales since their dynamics are not reliable. Further, as shown here, the large scales are affected negatively by interaction with the erroneous highly dispersive scales, though perhaps this could be addressed through refinements to the subgrid model. Whether explicitly filters are used or not, the effective range of dynamically resolved

scales is not defined by the grid spacing, but rather the dispersive properties of the numerical approximation to the convection term.

Appendix

1. Numerical representation of the vorticity-velocity formulation

The vorticity-velocity formulation introduced by Kim *et al.* [5] (referred to as KMM below) is a convenient way to solve the filtered or unfiltered Navier-Stokes equations when boundary conditions in two spatial directions (say x_1 and x_3) are periodic, and the numerical resolution in those directions is uniform. However, there is a subtlety to the formulation that arises when the discrete second derivative operator is not equivalent to the the discrete first derivative applied twice.

In the KMM formulation, the curl and the double curl operators are applied to the momentum equations, to obtain equations for the vorticity and the Laplacian of the velocity. The 2-component is then solved for, and a complete representation of the velocity is obtained from continuity. This formulation relies on three identities from vector calculus, which must also be satisfied by the discrete operators. Let $\tilde{\nabla}\cdot$, $\tilde{\nabla}$, $\tilde{\nabla}\times$ and $\tilde{\Delta}$ be the discrete divergence, gradient, curl and Laplacian operators, respectively. To recover the property of the KMM formulation that the pressure is eliminated, we must have

$$\tilde{\nabla} \times \tilde{\nabla}\psi = 0 \tag{A.1}$$

for any scalar field ψ. Further, to obtain the simple form used in KMM for the double curl of the momentum equation, and to reconstruct the full velocity,

$$\tilde{\nabla} \times \tilde{\nabla} \times \mathbf{A} = -\tilde{\nabla} \cdot \tilde{\nabla}\mathbf{A} + \tilde{\nabla}\tilde{\nabla} \cdot \mathbf{A} \tag{A.2}$$

must hold for any vector field $\mathbf{A}$, which ensures that the second term on the right will be zero when $\tilde{\nabla} \cdot \mathbf{A} = 0$. Both these discrete identities hold provided the same one-dimensional discrete derivatives are used to define the discrete divergence, gradient and curl operators. Finally, in KMM the 2-component of the double curl of the momentum equation yields an equation for ϕ, defined as the Laplacian of u_2, which requires that the discrete Laplacian obey $\tilde{\Delta}u_2 = \tilde{\nabla} \cdot \tilde{\nabla}u_2$, which is not generally true. So, instead, we define $\phi = \tilde{\nabla} \cdot \tilde{\nabla}u_2$.

Consider the discrete momentum and continuity equations:

$$\frac{\partial \mathbf{u}}{\partial t} = -\tilde{\nabla}p + \mathbf{H} \tag{A.3}$$

$$\tilde{\nabla} \cdot \mathbf{u} = 0 \tag{A.4}$$

which could be the Navier-Stokes equations (e.g. for a DNS) or the filtered Navier-Stokes equations (for an LES), in which case $\mathbf{u}$ is the filtered velocity. The $\mathbf{H}$ term includes the nonlinear, viscous and model (for LES) terms. Let $\tilde{\nabla}_p\cdot$ and $\tilde{\nabla}_p$ be the divergence and gradient operators restricted to the (1,3) plane, and let $\omega_2 = (\tilde{\nabla} \times \mathbf{u})_2$. Then the discrete version of the KMM formulation is given by

$$\frac{\partial \phi}{\partial t} = -\tilde{\nabla} \times \tilde{\nabla} \times \mathbf{H} \tag{A.5}$$

$$\frac{\partial \omega_2}{\partial t} = \tilde{\nabla} \times \mathbf{H} \tag{A.6}$$

$$\tilde{\nabla} \cdot \tilde{\nabla}u_2 = \phi \tag{A.7}$$

$$\tilde{\nabla}_p \cdot \tilde{\nabla}_p u_1 = \left(\frac{\delta \omega_2}{\delta x_3} - \frac{\delta}{\delta x_1}\frac{\delta u_2}{\delta y} \right) \tag{A.8}$$

$$\tilde{\nabla}_p \cdot \tilde{\nabla}_p u_3 = \left(\frac{\delta \omega_2}{\delta x_1} - \frac{\delta}{\delta x_3}\frac{\delta u_2}{\delta y} \right) \tag{A.9}$$

With periodic boundary conditions and uniform resolution in the x_1 and x_3 directions, the discrete derivative operators in those directions are circulant matrices, so that given ϕ and ω_2, (A.7-A.9) can be easily solved using discrete Fourier transforms, which is what makes the KMM formulation efficient. This also allows one to show that the solution for $\mathbf{u}$ so obtained does indeed satisfy $\tilde{\nabla}\cdot\mathbf{u} = 0$. The operators $\tilde{\nabla}\cdot\tilde{\nabla}$ and $\tilde{\nabla}_p\cdot\tilde{\nabla}_p$ that must be solved to recover the velocities using (A.7-A.9) are in general rank deficient because eigenvalues associated with the Nyquist modes are zero. This is

the property that leads to checkerboard instabilities in projection methods [31]. Here, the resulting singularity of the equations is resolved by insisting that all the Nyquist modes are zero, consistent with the Fourier cutoff filters used in the LES. Finally, we note that for spatial directions with periodic boundary conditions and uniform resolution, there is generally no motivation to use other than Fourier spectral representations. Non-spectral methods are used here only to allow the impacts of dispersion errors to be assessed, since often an LES must be conducted for boundary conditions and resolutions for which Fourier spectral methods are not practical.

The modified KMM formulation described here is designed to ensure that the solutions obtained satisfy the discrete filtered or unfiltered Navier-Stokes equations (A.3)-(A.4). This is important in the current study because we are interested in the effects of dispersion error in these equations, which are usually solved in practical simulations. However, it is also possible to derive the ϕ and ω_2 equations from the momentum and mass conservation equations before discretization, and then discretize them [3, 5]. In this case, the results are still numerical approximations to solutions of the conservation equations, but the numerical errors are different from those obtained by solving the discrete conservation equations.

2. Energy transfer rate for different forms of the nonlinear terms

Four different forms of the nonlinear terms are commonly used for numerical discretization of the filtered or unfiltered Navier-Stokes equations. While they are equivalent analytically, they are not equivalent in the presence of discretization error, and so result in different forms of the discrete energy transfer spectra. These forms and associated transfer spectra are listed below, with $\delta_j \equiv \frac{\delta}{\delta x_j}$, and u_i representing the filtered or unfiltered velocity, depending on whether the equations being solved are filtered.

1. Conservative form, $\delta_j(u_j u_i)$:

$$T_{\text{cons}}(\boldsymbol{\kappa},t) = -\text{Im}\left\{\sum_{\boldsymbol{\kappa}'} \tilde{\kappa}_\ell \hat{u}_k(\boldsymbol{\kappa},t)\hat{u}_k^*(\boldsymbol{\kappa}',t)\hat{u}_\ell^*(\boldsymbol{\kappa}-\boldsymbol{\kappa}',t)\right\} \tag{A.10}$$

2. Convective form, $u_j\delta_j(u_i)$:

$$T_{\text{conv}}(\boldsymbol{\kappa},t) = -\text{Im}\left\{\sum_{\boldsymbol{\kappa}'} \widetilde{\kappa'_\ell} \hat{u}_k(\boldsymbol{\kappa},t)\hat{u}_k^*(\boldsymbol{\kappa}',t)\hat{u}_\ell^*(\boldsymbol{\kappa}-\boldsymbol{\kappa}',t)\right\} \tag{A.11}$$

3. Skew-Symmetric form, $\frac{1}{2}\left(\delta_j(u_j u_i) + u_j\delta_j(u_i)\right)$:

$$T_{\text{skew}}(\boldsymbol{\kappa},t) = -\frac{1}{2}\text{Im}\left\{\sum_{\boldsymbol{\kappa}'} (\widetilde{\kappa'_\ell} + \tilde{\kappa}_\ell) \hat{u}_k(\boldsymbol{\kappa},t)\hat{u}_k^*(\boldsymbol{\kappa}',t)\hat{u}_\ell^*(\boldsymbol{\kappa}-\boldsymbol{\kappa}',t)\right\} \tag{A.12}$$

4. Rotational form, $u_j\delta_j(u_i) - u_j\delta_i(u_j) + \frac{1}{2}\delta_i(u_j u_j)$:

$$T_{\text{rot}}(\boldsymbol{\kappa},t) = -\text{Im}\left\{\sum_{\boldsymbol{\kappa}'} \widetilde{\kappa'_\ell} \hat{u}_k(\boldsymbol{\kappa},t)\hat{u}_k^*(\boldsymbol{\kappa}',t)\hat{u}_\ell^*(\boldsymbol{\kappa}-\boldsymbol{\kappa}',t) - \widetilde{\kappa'_k} \hat{u}_k(\boldsymbol{\kappa},t)\hat{u}_\ell^*(\boldsymbol{\kappa}',t)\hat{u}_\ell^*(\boldsymbol{\kappa}-\boldsymbol{\kappa}',t)\right\} \tag{A.13}$$

Since analytically the transfer spectrum $T(\boldsymbol{\kappa},t)$ is responsible for transferring energy between resolved modes, we expect $\sum_{\boldsymbol{\kappa}} T(\boldsymbol{\kappa},t) = 0$ for all t, reflecting conservation of energy. However, it is well known that in the presence of discretization error, both the conservative and convective forms do not satisfy this condition. To analyze this error, let $\tau_\ell(\boldsymbol{\kappa},\boldsymbol{\kappa}',t) = \hat{u}_k(\boldsymbol{\kappa},t)\hat{u}_k^*(\boldsymbol{\kappa}',t)\hat{u}_\ell^*(\boldsymbol{\kappa}-\boldsymbol{\kappa}',t)$. Then since $\tau_\ell(\boldsymbol{\kappa},\boldsymbol{\kappa}',t) = \tau_\ell(-\boldsymbol{\kappa}',-\boldsymbol{\kappa},t)$ we can write

$$\sum_{\boldsymbol{\kappa}} T_{\text{cons}}(\boldsymbol{\kappa},t) = -\text{Im}\left\{\sum_{\boldsymbol{\kappa}}\sum_{\boldsymbol{\kappa}'} \tilde{\kappa}_\ell \tau_\ell(\boldsymbol{\kappa},\boldsymbol{\kappa}',t)\right\} = -\frac{1}{2}\text{Im}\left\{\sum_{\boldsymbol{\kappa}}\sum_{\boldsymbol{\kappa}'} (\tilde{\kappa}_\ell - \widetilde{\kappa'_\ell})\tau_\ell(\boldsymbol{\kappa},\boldsymbol{\kappa}',t)\right\}. \tag{A.14}$$

Moreover, $\widetilde{(\kappa-\kappa')}_\ell \tau_\ell(\boldsymbol{\kappa},\boldsymbol{\kappa}',t) = 0$ by continuity. Therefore,

$$\sum_{\boldsymbol{\kappa}} T_{\text{cons}}(\boldsymbol{\kappa},t) = -\frac{1}{2}\text{Im}\left\{\sum_{\boldsymbol{\kappa}}\sum_{\boldsymbol{\kappa}'} \left(\tilde{\kappa}_\ell - \widetilde{\kappa'_\ell} - \widetilde{(\kappa-\kappa')}_\ell\right) \hat{u}_k(\boldsymbol{\kappa},t)\hat{u}_k^*(\boldsymbol{\kappa}',t)\hat{u}_\ell^*(\boldsymbol{\kappa}-\boldsymbol{\kappa}',t)\right\}. \tag{A.15}$$

Similarly, for the convective form,

$$\sum_{\boldsymbol{\kappa}} T_{\mathrm{conv}}(\boldsymbol{\kappa},t) = -\frac{1}{2}\mathrm{Im}\left\{\sum_{\boldsymbol{\kappa}}\sum_{\boldsymbol{\kappa}'}\left(\widetilde{\kappa'_\ell} - \tilde{\kappa}_\ell + \widetilde{(\kappa-\kappa')}_\ell\right)\hat{u}_k(\boldsymbol{\kappa},t)\hat{u}_k^*(\boldsymbol{\kappa}',t)\hat{u}_\ell^*(\boldsymbol{\kappa}-\boldsymbol{\kappa}',t)\right\}. \tag{A.16}$$

For numerical methods other than Fourier spectral, $\tilde{\boldsymbol{\kappa}}$ is a nonlinear function of $\boldsymbol{\kappa}$, so $\tilde{\boldsymbol{\kappa}} - \widetilde{\boldsymbol{\kappa}'} - \widetilde{(\boldsymbol{\kappa}-\boldsymbol{\kappa}')} \neq 0$. Therefore, the violation of conservation of energy for the conservative and convective forms can be directly attributed to the fact that the effective wavenumbers of triad interacting wavemodes do not sum to zero, as was the case for the effects of dispersion due to mean convection (see Eq. 9). Notice that the errors given by (A.15) and (A.16) are equal and opposite and so $\sum_{\boldsymbol{\kappa}} T_{\mathrm{skew}}(\boldsymbol{\kappa},t) = 0$ as expected. Similarly, the rotational form is energy conserving by construction so $\sum_{\boldsymbol{\kappa}} T_{\mathrm{rot}}(\boldsymbol{\kappa},t) = 0$. Finally, note that the contribution of mean convection to the nonlinear terms is the same in all four forms, regardless of discretization error. Therefore, the effects of mean convection are the same and the analysis in equations (6)-(9) holds for each form.

ACKNOWLEDGMENTS

The authors acknowledge the generous financial support from the National Aeronautics and Space Administration (cooperative agreement number NNX15AU40A), the National Science Foundation (project number 1904826), and the U.S. Department of Energy, Exascale Computing Project (subcontract number XFC-7-70022-01 from contract number DE-AC36-08GO28308 with the National Renewable Energy Laboratory). Thanks are also due to the Texas Advanced Computing Center at The University of Texas at Austin for providing HPC resources that have contributed to the research results reported here.

[1] R. D. Moser, S. W. Haering, and G. R. Yalla, Statistical properties of subgrid-scale turbulence models, Annual Review of Fluid Mechanics **53**, 255 (2021).
[2] G. R. Yalla, T. A. Oliver, S. W. Haering, B. Engquist, and R. D. Moser, Effects of resolution inhomogeneity in large-eddy simulation, Physical Review Fluids **6**, 074604 (2021).
[3] M. Lee and R. D. Moser, Direct numerical simulation of turbulent channel flow up to $Re_\tau \approx 5200$, Journal of Fluid Mechanics **774**, 395 (2015).
[4] P. R. Spalart, R. D. Moser, and M. M. Rogers, Spectral methods for the navier-stokes equations with one infinite and two periodic directions, Journal of Computational Physics **96**, 297 (1991).
[5] J. Kim, P. Moin, and R. Moser, Turbulence statistics in fully developed channel flow at low reynolds number, Journal of Fluid Mechanics **177**, 133 (1987).
[6] T. A. Zang, On the rotation and skew-symmetric forms for incompressible flow simulations, Applied Numerical Mathematics **7**, 27 (1991).
[7] E. Tadmor, Skew-selfadjoint form for systems of conservation laws, Journal of Mathematical Analysis and Applications **103**, 428 (1984).
[8] F. K. Chow and P. Moin, A further study of numerical errors in large-eddy simulations, Journal of Computational Physics **184**, 366 (2003).
[9] G. Blaisdell, E. Spyropoulos, and J. Qin, The effect of the formulation of nonlinear terms on aliasing errors in spectral methods, Applied Numerical Mathematics **21**, 207 (1996).
[10] P. Mohan, N. Fitzsimmons, and R. D. Moser, Scaling of lyapunov exponents in homogeneous isotropic turbulence, Physical Review Fluids **2**, 114606 (2017).
[11] S. A. Orszag, On the elimination of aliasing in finite-difference schemes by filtering high-wavenumber components, Journal of the Atmospheric Sciences **28**, 1074 (1971).
[12] D. Leslie and G. Quarini, The application of turbulence theory to the formulation of subgrid modelling procedures, Journal of fluid mechanics **91**, 65 (1979).
[13] S. W. Haering, M. Lee, and R. D. Moser, Resolution-induced anisotropy in large-eddy simulations, Physical Review Fluids **4**, 114605 (2019).
[14] C. Cambon, N. N. Mansour, and F. S. Godeferd, Energy transfer in rotating turbulence, Journal of Fluid Mechanics **337**, 303 (1997).
[15] F. Waleffe, Inertial transfers in the helical decomposition, Physics of Fluids A: Fluid Dynamics **5**, 677 (1993).
[16] The lower order approximations do not have a wide enough range of non-dispersive scales for the scaling to hold.
[17] D. Coles, The law of the wake in the turbulent boundary layer, Journal of Fluid Mechanics **1**, 191 (1956).
[18] F. Porté-Agel, M. Bastankhah, and S. Shamsoddin, Wind-turbine and wind-farm flows: a review, Boundary-Layer Meteorology **174**, 1 (2020).

[19] S. Ghosal, An analysis of numerical errors in large-eddy simulations of turbulence, Journal of Computational Physics **125**, 187 (1996).
[20] A. Kravchenko and P. Moin, On the effect of numerical errors in large eddy simulations of turbulent flows, Journal of Computational Physics **131**, 310 (1997).
[21] T. Lund, The use of explicit filters in large eddy simulation, Computers & Mathematics with Applications **46**, 603 (2003).
[22] D. Carati, G. S. Winckelmans, and H. Jeanmart, On the modelling of the subgrid-scale and filtered-scale stress tensors in large-eddy simulation, Journal of Fluid Mechanics **441**, 119 (2001).
[23] J. Gullbrand and F. K. Chow, The effect of numerical errors and turbulence models in large-eddy simulations of channel flow, with and without explicit filtering, Journal of Fluid Mechanics **495**, 323 (2003).
[24] G. S. Winckelmans, A. A. Wray, O. V. Vasilyev, and H. Jeanmart, Explicit-filtering large-eddy simulation using the tensor-diffusivity model supplemented by a dynamic smagorinsky term, Physics of Fluids **13**, 1385 (2001).
[25] M. Germano, Differential filters for the large eddy numerical simulation of turbulent flows, The Physics of Fluids **29**, 1755 (1986).
[26] H. van der Ven, A family of large eddy simulation (LES) filters with nonuniform filter widths, Physics of Fluids **7**, 1171 (1995).
[27] O. V. Vasilyev, T. S. Lund, and P. Moin, A general class of commutative filters for les in complex geometries, Journal of Computational Physics **146**, 82 (1998).
[28] A. L. Marsden, O. V. Vasilyev, and P. Moin, Construction of commutative filters for les on unstructured meshes, Journal of Computational Physics **175**, 584 (2002).
[29] S. T. Bose, P. Moin, and D. You, Grid-independent large-eddy simulation using explicit filtering, Physics of Fluids **22**, 105103 (2010).
[30] S. Bose, P. Moin, and F. Ham, Explicitly filtered large eddy simulation on unstructured grids, Annual Research Briefs, Center for Turbulence Research , 87 (2011).
[31] F. H. Harlow and J. E. Welch, Numerical calculation of time-dependent viscous incompressible flow of fluid with free surface, The Physics of Fluids **8**, 2182 (1965).